



Relative positioning of formation-flying spacecraft using single-receiver GPS carrier phase ambiguity fixing

Gerardo Allende-Alba¹ · Oliver Montenbruck¹ · Stefan Hackel¹ · Michel Tossaint²

Received: 22 November 2017 / Accepted: 23 April 2018 / Published online: 2 May 2018
© Springer-Verlag GmbH Germany, part of Springer Nature 2018

Abstract

In recent years, differential carrier phase-based relative positioning (or “baseline determination”) with precision at the millimeter and submillimeter levels has been demonstrated for the GRACE, TanDEM-X and Swarm missions in offline processing. Specific features of such missions have included the use of spacecraft of similar shapes placed in almost identical orbits as well as the use of consistent geodetic-class GPS receivers. These elements have proven to be advantageous for the computation of baseline solutions with such precision levels. Particularly, they have allowed to fully leverage the use of differential GPS techniques, including the estimation and use of carrier phase integer ambiguities. Similarly, the aforementioned spacecraft and orbit characteristics have made it possible to tightly constrain the relative dynamics of formations in the generation of reduced-dynamic solutions. Other than the former examples, prospective formation-flying mission proposals, such as SAOCOM-CS and PICOSAR, may comprise spacecraft with very different characteristics, including dissimilar GPS/GNSS receivers. Such cases may no longer provide favorable conditions for relative orbit determination strategies. As an alternative, absolute orbit solutions may be computed individually for each spacecraft and used for the generation of precise baseline products. This study aims at the assessment of the potential of single-receiver ambiguity fixing for the generation of precise baseline solutions. Results using flight data from the GRACE, TanDEM-X and Swarm missions exhibit baseline accuracy better than 5 mm (3D RMS) for a one-month test period in June 2016. As such, the presented solutions may be considered for prospective formation-flying remote sensing missions with baseline precision requirements at the subcentimeter level. Likewise, the method is considered of particular interest for future multi-spacecraft formations and swarms that require efficient determination of a large number of individual baselines.

Keywords Single-receiver ambiguity fixing · Precise baseline determination · Formation-flying spacecraft · Relative positioning

Introduction

The potential of spacecraft formation-flying missions to provide enhanced capabilities for earth observation has been demonstrated in various missions over the past years. Prominent examples operating in the low earth orbit (LEO) include the GRACE (Tapley et al. 2004), TanDEM-X (Krieger et al. 2007) and Swarm (Friis-Christensen et al. 2008) missions.

Depending on the specific application, the generation of remote sensing products may require the computation of offline baseline solutions with varying precision requirements. A well-known example is the interferometric synthetic aperture radar (InSAR) technique implemented in the TanDEM-X mission, which set a baseline precision requirement of 1 mm (1D RMS) for the generation of a global digital elevation model (DEM; Krieger et al. 2013). This particularly challenging requirement could be substantially fulfilled mostly by employing precise baseline determination systems using carrier phase differential GPS (CDGPS) observations with fixed integer ambiguities (Montenbruck et al. 2011; Hueso González et al. 2012).

In all of the aforementioned examples, special mission/spacecraft characteristics were of fundamental importance for the attainment of baseline precision at the millimeter

✉ Gerardo Allende-Alba
gerardo.allendealba@dlr.de

¹ Deutsches Zentrum für Luft und Raumfahrt (DLR), German Space Operations Center (GSOC), 82230 Weßling, Germany

² European Space Agency (ESA), European Space Research and Technology Centre (ESTEC), 2201 Noordwijk, Netherlands

and submillimeter levels. Among these, the use of common geodetic-class GPS receivers with zenith pointing antennas were key factors for leveraging the implementation of CDGPS techniques. Additionally, in such mission profiles with spacecraft of equal geometric structure and almost identical orbits, the generation of reduced-dynamic baseline solutions typically benefits from the application of tight relative dynamics constraints.

Although various planned formation-flying missions such as GRACE-FO (Flechtner et al. 2014) and TanDEM-L (Moreira et al. 2015) will inherit many design elements from their predecessors, alternative mission concepts have recently started to be considered for implementation of extended remote sensing techniques. Among these, multiple-aperture sensing may open the possibility for a variety of applications, including multi-baseline DEM generation (Krieger and Moreira 2008) and SAR tomography (Homer et al. 1996). In various SAR mission concepts, semi-active configurations have been contemplated, consisting of a main spacecraft as illuminator and one or more passive receivers, comprised different (e.g., smaller) spacecraft platforms (Krieger and Moreira 2006). Notable examples of prospective and planned missions with related characteristics include SAOCOM-CS (Barbier et al. 2014), Garada (Qiao et al. 2011) and PICOSAR (Börner et al. 2014).

Due to the expected increase of complexity in future remote sensing mission concepts, current strategies for baseline determination may turn out to be inadequate for specific mission profiles. In particular, the computation of baseline solutions based on dual-spacecraft strategies (Jäggi et al. 2007; Kroes et al. 2005) may result impractical if the number of spacecraft (and hence baselines) increases. Likewise, when spacecraft of different characteristics are considered, the relative dynamics of the formation cannot be tightly constrained in the computation of reduced-dynamic solutions. Furthermore, dissimilar spacecraft designs (particularly GNSS antenna positioning/alignment) and/or selected formation geometries may lead to unfavorable tracking conditions that are less suitable for application of CDGPS techniques. Even if the considered GNSS receivers can guarantee carrier phase integer ambiguities, the difficulty to apply differential processing techniques may prevent the successful application of integer ambiguity resolution strategies. As a result, even dedicated processing strategies for multi-spacecraft baseline determination may experience a reduced performance under the consideration of such cases (van Barneveld 2012).

In an effort to cope with the various challenges for precise baseline determination (PBD) in multi-satellite formation-flying missions, the present study evaluates the potential of single-satellite precise orbit determination (POD) for the generation of baseline solutions. A key feature of the GPS-based POD technique is its maturity,

as it has served as a chief source of orbit information for numerous remote sensing and earth observation missions in LEO (Bertiger et al. 1994; Bock et al. 2014, 2017; Haines et al. 2004; Kang et al. 2006; van den Ijssel et al. 2003, 2015). Typical POD schemes make use of GPS carrier phase observations with float ambiguities. Solutions resulting from such a strategy can be used for the generation of baseline products with representative accuracies at the 1–2 cm level (3D RMS) (Montenbruck et al. 2011).

On the other hand, the use of the precise point positioning with ambiguity resolution (PPP-AR) concept (Tennisen and Khodabandeh 2015) for the improvement of POD products has been recently explored. Laurichesse and Mercier (2007) introduced at the French Space Agency (CNES) the implementation of single-receiver ambiguity fixing techniques and their application to orbit determination of satellites in LEO. As a result, it was shown that an overall improvement of precise orbit solutions could be attained (Laurichesse et al. 2009). A similar strategy was subsequently implemented at the Jet Propulsion Laboratory (JPL), which in turn was incorporated into the routine generation of orbit products with improved accuracy (Bertiger et al. 2010). In these analyses, the performance of baseline solutions generated with ambiguity fixed POD (POD-AR) products could be assessed by employing data from the GRACE mission. Using observations from the K/Ka-band ranging (KBR) instrument as a reference, Laurichesse et al. (2009) and Bertiger et al. (2010) demonstrated a baseline precision of 2 mm (1D, 1σ) using data from 2003 to 2009, respectively.

Aside from the above-mentioned maturity of POD methods, an important advantage of the POD-AR approach is that baseline solutions can be generated in independent processing chains. This feature may be especially attractive for prospective remote sensing missions based on multi-spacecraft formations or aggregated designs considering diverse spacecraft platforms (e.g., from different space agencies).

The present study is devoted to the performance evaluation of precise baseline solutions based on POD-AR products considering all three dimensions and using a wider set of missions than available before. Following a description of the strategies and models used for POD, we briefly present the employed strategy for single-receiver integer ambiguity resolution and the generation of POD-AR solutions. Subsequently, a description of precise baseline products used as reference for assessment of solutions is presented. Finally, we evaluate and discuss the accuracy of the generated POD-AR baseline solutions. For this purpose, flight data from the GRACE, TanDEM-X and Swarm missions have been used in order to test the presented strategies under different formation-flying mission profiles and GPS receiver characteristics.

Precise orbit determination

The quality of POD solutions is largely driven by the choice and complexity of models for the satellite motion and the GNSS observations. Relevant models employed in the present study are described in the sequel and summarized in Table 1.

Dynamical models

The employed dynamical models take into account both gravitational and non-gravitational accelerations. Unlike gravitational forces, which can be modeled to act on the spacecraft's center-of-mass, non-gravitational forces are surface-dependent and hence require information about the spacecraft geometric structure. In the present study, high-fidelity models are used for the description of gravitational forces whereas a macro-model formulation is considered for

Table 1 Models and methods used for the computation of precise orbit and baseline solutions

	POD-AR	PBD-1	PBD-2
GPS observation model	Undifferenced ionosphere-free code and carrier phase combinations CNES/CLS GRG and widelane bias products ^a IGS igs08.atx ^c transmitter antenna phase center offset and variations Mission-specific receiver antenna phase center offset and in-flight calibrated phase variations Carrier phase wind-up ^d 30 s sampling	Single-difference (between receivers) ionosphere-free code and carrier phase combinations CODE final products ^b	
Integer ambiguity resolution	Pass-by-pass single-receiver widelane and N1 ambiguity fixing ^e using CNES/CLS widelane and clock products ^a	Pass-by-pass single-difference (between receivers) widelane and N1 ambiguity fixing	Sliding batches N1 and N2 ambiguity fixing ^f
Dynamical model	GOCO03S earth's gravity field model (100×100) ^g . Linear drift of C_{20} , C_{21} , S_{21} Luni-solar perturbations (analytical series) Solid earth and pole tides (IERS2003) Ocean tides (CSR/Topex3.0) ^h Post-Newtonian corrections Macro-model for atmospheric forces (using NRLMSISE-00 density model ⁱ), solar radiation pressure (using conical earth shadow model ^j) and earth radiation pressure (using CERES earth radiation data ^k) Thrust arcs and empirical accelerations in radial, tangential and normal direction		
Reference frames	ICRF, IGB08 (earth orientation parameters from IGS. IERS1996 conventions)		
Numerical integration	Variable-order variable step-size multistep Shampine–Gordon method ^l		Fourth-order Runge–Kutta method
Estimation	Batch least-squares Estimation of piece-wise constant (10 min intervals) empirical accelerations Estimation of constant thrust arcs		Extended Kalman filter Estimation of epoch-wise differential empirical accelerations with exponential time correlation Applied thrust arcs with increase of process noise

^aLoyer et al. (2012)

^bDach et al. (2009)

^cSchmid et al. (2016)

^dWu et al. (1993)

^eMontenbruck et al. (2017)

^fAllende-Alba and Montenbruck (2016)

^gMayer-Gürr et al. (2012)

^hEanes and Bettadpur (1996)

ⁱPicone et al. (2002)

^jMontenbruck and Gill (2005)

^kPriestley et al. (2011)

^lShampine and Gordon (1975)

the computation of accelerations due to atmospheric forces and radiation pressure (Hackel et al. 2017). The spacecraft geometry is approximated in the macro-models by means of surface descriptors, including size, orientation, and optical properties.

Accelerations due to atmospheric forces, comprising drag and lift, are computed for each spacecraft surface using the implementation of Sutton (2009) and Doornbos (2012) of the Sentman's model (Sentman 1961). Atmospheric composition and density data are computed using the US Naval Research Laboratory Mass Spectrometer and Incoherent Scatter Radar 2000 (NRLMSISE-00) model (Picone et al. 2002). Daily solar radio flux F10.7 and 3-h geomagnetic Kp indices are obtained from the Space Weather Prediction Center of the National Oceanic and Atmospheric Administration (NOAA).

Accelerations due to radiation pressure make use of parameters included in macro-models, which characterize radiation properties of the spacecraft surfaces. These parameters describe the fraction of photons that are absorbed and reflected (diffusely and specularly) on each illuminated surface. For the case of solar radiation pressure, the respective accelerations are computed considering photons in the visible spectrum based on the model of Milani et al. (1987). Sun illumination conditions (e.g., umbra/penumbra) are considered by using a conical shadow model for a spherical Earth. For the case of earth radiation pressure, solar photons reflected by the earth crust and photons from thermal radiation of the earth are taken into account based on the approach of Knocke et al. (1988). Earth albedo and emissivity data are provided by the Clouds and Earth's Radiant Energy System (CERES; Priestley et al. 2011).

Although the described models provide a very good approximation of the spacecraft dynamics in LEO, uncertainties in the employed data and spacecraft parameterization lead to unmodeled accelerations. To compensate for residual accelerations due to atmospheric forces, solar and earth radiation pressure, a set of three global scaling parameters and complementary empirical accelerations are adjusted in the orbit determination process.

Observation models

The POD-AR solutions generated for this study make use of GPS dual-frequency ionosphere-free code and carrier phase observations. Absolute phase center offsets (PCO) and variations (PV) for transmitting GPS antennas have been obtained from the IGS solution (Schmid et al. 2016). For the S67-1575-14+CRG GPS antennas used in the GRACE and TanDEM-X missions, on-ground and in-flight calibrated absolute PCOs and PVs have been used (Montenbruck et al. 2009). For the Swarm spacecraft, in-flight calibrated PVs without additional PCOs have been considered. Precise GPS

orbit and clock products from the CNES/Collecte Localisation Satellites (CLS) analysis center were employed (Loyer et al. 2012). The phase wind-up effect on carrier phase observations has been modeled according to Wu et al. (1993).

Estimation scheme

For the computation of precise orbit solutions considered in this study, the employed strategy is based on the reduced-dynamic approach (Wu et al. 1991; Yunck et al. 1990). The previously described dynamical models are complemented by the estimation of piece-wise constant (10-min intervals) empirical accelerations in the radial, along-track and cross-track directions. Similarly, orbit control maneuvers are taken into account as constant thrust arcs in the three orbital components.

The estimation scheme consists of a batch least-squares adjustment of epoch-wise receiver clock offsets, the initial state vector, scale factors for the employed dynamical models, orbit control maneuvers, empirical accelerations as well as pass-wise ionosphere-free carrier phase biases. Orbit solutions are obtained for 24-h observation batches.

Flight data

For the present study, a 30-day data set covering the period of June 2016 for the GRACE, TanDEM-X and Swarm missions was used to validate the presented strategies. For the GRACE mission, the publicly available Level 1B data from the Physical Oceanography Distributed Active Archive Center (PODAAC; PODAAC 2017) of the Jet Propulsion Laboratory (JPL) were used. Flight data from the TanDEM-X mission were provided by the GeoForschungsZentrum (GFZ) Potsdam. For the Swarm mission, data were made available by the European Space Agency (ESA) within the frame of the data quality working group. Raw GPS data from the GPSR instruments were used for the generation of RINEX files with carrier phase half-cycle correction, according to the procedure described by Montenbruck et al. (2017). Table 2 provides an overview of the missions considered in this study.

Single-receiver integer ambiguity resolution

A key feature of the strategy for POD employed in this study is the capability of single-receiver integer ambiguity resolution and thus the generation of POD-AR solutions. This is enabled by dedicated GPS clock products and network-calibrated widelane biases generated by the CNES/CLS data center (Loyer et al. 2012). The employed ambiguity resolution strategy is based on Laurichesse et al.

Table 2 Formation-flying missions considered in this study as test cases

Mission	Spacecraft	Approximate baseline dimension [km]	GPS receiver (manufacturer)
GRACE	GRACE A/GRACE B	220	BlackJack (JPL)
TanDEM-X	TSX/TDX	< 1	IGOR (Broadreach)
Swarm	Swarm A/Swarm C	60–175	GPSR (RUAG)

(2009) and further described in Montenbruck et al. (2017). It consists of a two-step approach in which the widelane and N1 ambiguities are resolved. First, observations are arranged according to continuous carrier phase tracking arcs (passes). For each observation epoch and tracked satellite, a (Hatch–)Melbourne–Wübbena (MW; Hatch1982; Melbourne1985; Wübbena1985) is formed. On each pass p , the averaged value \overline{MW}^p of the MW combination (expressed in widelane cycles) is corrected by using satellite-specific fractional widelane biases $\mu_{WL}^{(i)}$ obtained from the CNES/CLS widelane satellite bias (WSB) product. The resulting value

$$\left(\overline{MW}^p + \mu_{WL}^{(i)}\right) = N_{WL}^p + \mu_{WL} + \epsilon_{MW} \tag{1}$$

can be expressed as the sum of a pass-specific integer ambiguity N_{WL}^p , a receiver-specific fractional widelane bias μ_{WL} and residual errors ϵ_{MW} of the pass-averaged MW combination. Estimates of pass-specific integer ambiguities N_{WL}^p and the common receiver bias μ_{WL} can be obtained as part of a mixed-integer problem (Montenbruck et al. 2017). Due to a typically moderate standard deviation $\sigma(\epsilon_{MW})$ close to 0.1 widelane cycles, a simple rounding estimator is deemed as suitable for the estimation of ambiguities. As an example, Fig. 1 depicts the widelane ambiguity residuals (float-integer) on a sample day for the GRACE A, TSX and Swarm A spacecraft.

In a second step, the estimated widelane ambiguities are used to improve the float ambiguity solution provided by the standard POD system. Within this scheme, float-valued pass-specific ionosphere-free biases β^p are estimated. These biases can be expressed as

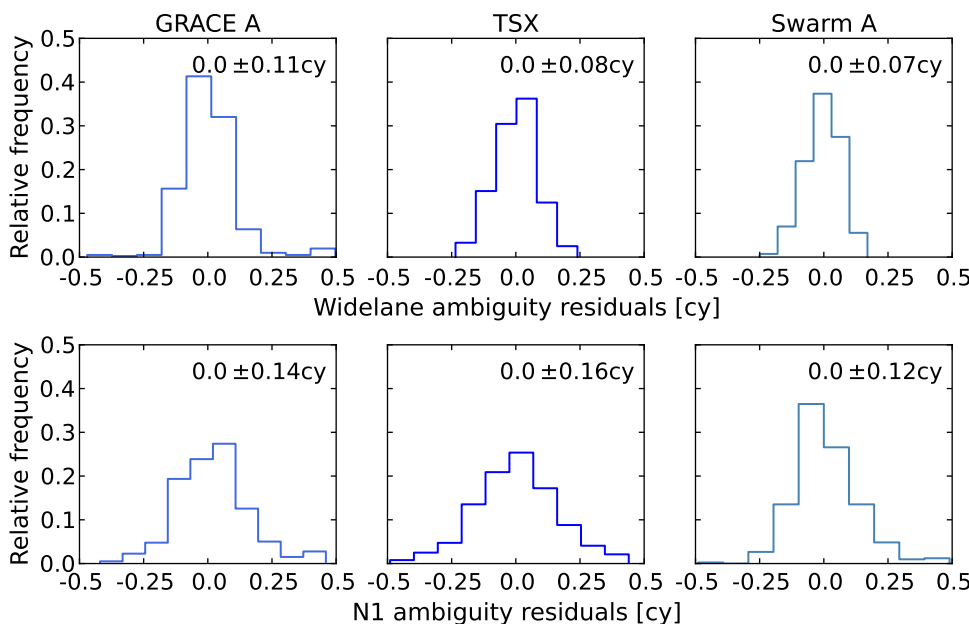
$$\beta^p = \lambda_{NL} \left(N_1^p + \frac{\lambda_{WL}}{\lambda_2} N_{WL}^p + b \right), \tag{2}$$

where λ_{WL} , λ_{NL} and λ_2 are the wavelengths of the widelane combination, the narrowlane combination and the L2 observations, respectively. Furthermore, N_1^p denotes the integer-valued ambiguity of the L1 observation and b is a float-valued bias. When working with the CNES/CLS clock products, which lump the satellite receiver clock offsets with satellite-specific fractional phase biases (Laurichesse et al. 2009; Loyer et al. 2012), b is nominally constant and common to all passes. Equation (2) can further be rearranged as

$$\frac{\beta^p}{\lambda_{NL}} - \frac{\lambda_{WL}}{\lambda_2} N_{WL}^p = N_1^p + b, \tag{3}$$

which enables estimation of N_1^p and b in a mixed-integer problem from observed values of β^p and the known widelane ambiguities N_{WL}^p .

Fig. 1 Frequency distribution of widelane (top) and N1 (bottom) ambiguity residuals (float-fixed) for an example data set from the GRACE A, TSX and Swarm A spacecraft on June 1, 2016



As discussed in Montenbruck et al. (2017), a major difficulty for this approach stems from the fact that the estimated values of β^p may be contaminated by time varying receiver biases or receiver clock offset contributions, so that b can no longer be assumed to be rigorously constant. However, the encountered variations are sufficiently slow to eliminate (or at least highly reduce) their impact when forming differences between adjacent passes. The difference $N_1^{pq} = N_1^p - N_1^q$ can thus be obtained with good confidence from the respective between-passes differences β^{pq} and N_{WL}^{pq} of the ionosphere-free pass biases and widelane ambiguities. A rounding estimator can again be used to estimate integer-valued N1 ambiguity differences and a swift validation strategy is employed based on testing of the ambiguity residuals against a pre-defined threshold. This strategy has been deemed adequate for the present scheme and test cases in view of the obtained standard deviation of ambiguity residuals below 0.2 narrowlane cycles (Fig. 1). Once ambiguities are fixed and accepted, a soft-constraint is applied to the orbit determination system in order to fix the values $(\beta)^{pq}$ in subsequent iterations of the POD process. In practice, 2 iterations with float ambiguity estimates and 2–3 subsequent iterations with integer resolution are used to obtain the final, ambiguity fixed POD solution.

Reference baseline solutions

For the assessment of the baseline solutions under evaluation, this study employs dedicated precise baseline products computed using differential carrier phase observations. The scheme, hereafter denoted as PBD-1, is built on the strategy described by Allende-Alba et al. (2017). It is based on the reduced-dynamic approach and makes use of single-difference ionosphere-free GPS observation models. The strategy consists of a batch least-squares estimation scheme, which is used to adjust relative epoch-wise receiver clock offsets, the relative initial state vector, differential scale factors for non-gravitational accelerations, relative empirical accelerations as well as pass-specific single-difference ionosphere-free carrier phase biases. Other than the approach used by Allende-Alba et al. (2017), ambiguity fixed solutions are obtained within the present study by resolving between-receiver widelane and N1 ambiguities on a pass-by-pass basis.

In the absence of references for the assessment of solutions from the PBD-1 scheme, an inter-product comparison using solutions from a second (algorithmically independent) scheme is performed in this study for that purpose. Such a scheme, hereafter denoted as PBD-2, is described in Allende-Alba and Montenbruck (2016). It makes use of a dedicated strategy for integer ambiguity resolution employing a so-called sliding batches approach. An a priori-constrained least-squares estimator is used for float ambiguity

estimation whereas integer least-squares [encoded in the LAMBDA algorithm (Teunissen 1994)] and integer aperture estimators are used for ambiguity estimation and validation. Fixed ambiguities are subsequently introduced as known values into a reduced-dynamic baseline determination system based on an extended Kalman filter.

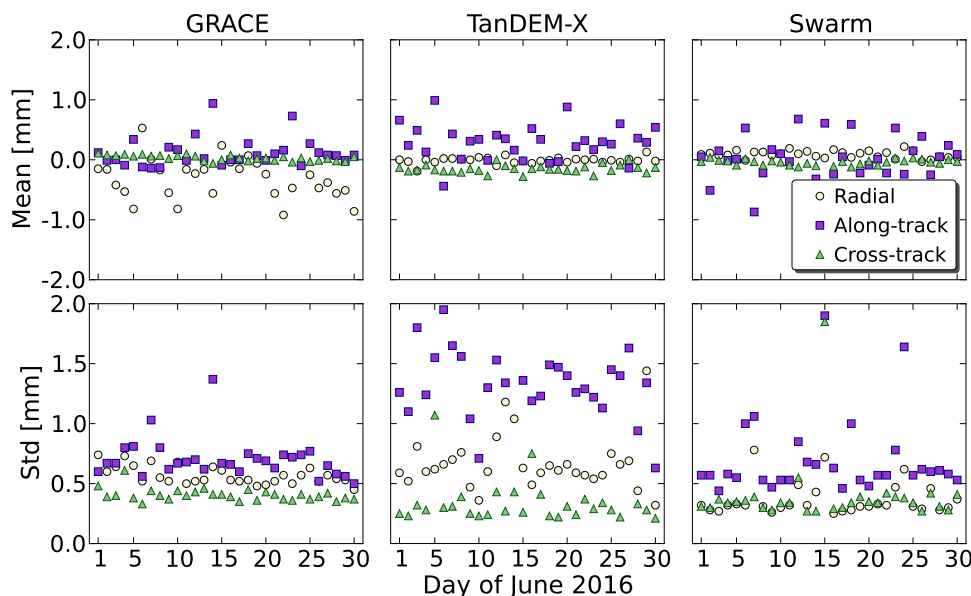
Within the filter, the relative trajectory of one spacecraft with respect to the other spacecraft is adjusted using a single-difference ionosphere-free observation model. At each observation epoch, the spacecraft relative trajectory is estimated together with relative receiver clock offsets, differential scale factors for non-gravitational accelerations, relative empirical accelerations as well as single-difference ionosphere-free carrier phase biases for current satellites in view. A summary of the models and strategies used in the PBD-1 and PBD-2 schemes is provided in Table 1.

Figure 2 depicts the consistency of reference baseline solutions computed with the PBD-1 and PBD-2 schemes for the three formation-flying missions and the period under analysis. In this assessment, one-hour data arcs centered at maneuver execution times have been excluded due to the maneuver handling strategy used in the PBD-2 scheme. In general, both types of solutions exhibit a consistency with daily biases below 1 mm and median biases lower than 0.5 mm for the three test cases. For the GRACE and Swarm missions, the baseline solutions show median values of the daily standard deviations below 1 mm in all three orbital components. For the case of TanDEM-X, similar consistency levels were obtained in the radial and cross-track directions. A slightly worse agreement was obtained in the along-track direction, exhibiting a median standard deviation of 1.3 mm. Probable causes of this slightly degraded performance of one or both reference solution types are under investigation. Nonetheless, the achieved general consistency level for the three test cases suggests the feasibility of using either of the two solutions as reference for assessment of the POD-AR baselines solutions. In the subsequent analysis, PBD-1 has been selected for this purpose.

Results and discussion

According to the methodology described in previous sections, the baseline solutions under analysis in this study were generated by differencing POD-AR solutions. Based on the quality of estimates of ionosphere-free float ambiguities (see Fig. 1), a threshold of 0.15 narrowlane cycles (≈ 1.6 cm) was used to validate fixed N1 ambiguities for the case of TanDEM-X and Swarm. A slightly larger threshold of 0.25 narrowlane cycles (≈ 2.6 cm) was used for GRACE data. This configuration was selected in order to decrease the false alarm rate in ambiguity rejection tests, which apparently was one of the main causes of baseline solutions with

Fig. 2 Inter-product consistency (top: mean value; bottom: standard deviation) of precise baseline solutions from the PBD-1 and PBD-2 schemes for the GRACE, TanDEM-X and Swarm missions in June 2016



degraded quality obtained during early tests for this study. The employed ambiguity validation thresholds resulted in widelane ambiguity fixing rates above 97% for the three missions under test. In the case of N1 ambiguities, the resulting fixing rates after the first ambiguity resolution iteration were of 85–90% for GRACE and Swarm, whereas for TanDEM-X they were around 70%. These values roughly reflect the number of ambiguities that can be fixed with enough confidence in the example distribution of residuals depicted in Fig. 1. Given that N1 fixed ambiguities from a first iteration are used to constrain the solution of the orbit determination problem in subsequent iterations, the stiffness of the resulting orbit is increased. As a consequence, estimates of remaining float ambiguities get improved, which allows increasing the number of fixed ambiguities in each iteration. After 2–3 ambiguity resolution iterations, representative fixing rates above 95% could be obtained for most of the days under analysis and the three test cases under consideration.

For an independent validation of POD-AR baseline solutions for the GRACE mission, observations from the KBR instrument have been used as reference. Figure 3 depicts the precision assessment of POD-AR baseline solutions in terms of KBR residuals. For comparison, the assessment of baseline solutions derived from the JPL’s GNV1B product is likewise depicted. Overall, the POD-AR baseline solutions from this study exhibit a two-fold better (1D, 1σ) precision with respect to their GNV1B counterpart. Median values of the daily standard deviations of the KBR residuals amount to 2.6 and 6.4 mm for our POD-AR solutions and the GNV1B product, respectively. As stated before, previous studies conducted at CNES (Laurichesse et al. 2009) and JPL (Bertiger et al. 2010) inferred a 2-mm (1D, 1σ) baseline precision using data from before 2010. However,

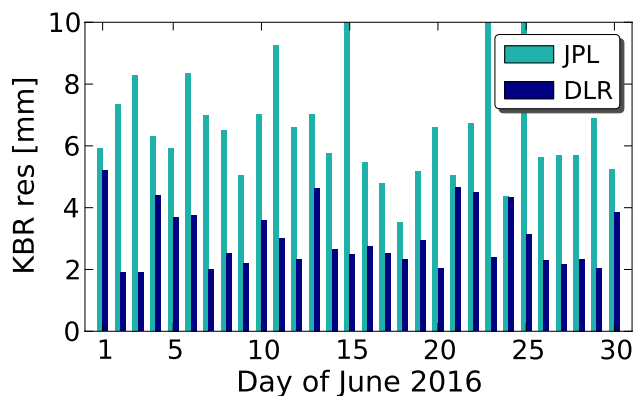


Fig. 3 Precision assessment in terms of KBR residuals of baseline solutions derived from the GNV1B (JPL) and POD-AR (DLR) products for the GRACE mission in June 2016

a more recent study by Mao et al. (2017) already reported a degradation of KBR residuals with baseline solutions from JPL’s GNV1B products down to 6 mm using data from 2014, which is in agreement with the value obtained in this study. In contrast, the POD-AR baseline solutions generated here exhibit only slightly worse precision levels (on average) than those reported in the early CNES and JPL studies based on data before 2010. It may be suspected that the observed performance degradation of the GNV1B product is related to the lower altitude and higher atmospheric drag, but might be removed through retuning of the operational POD process.

A more general assessment method is carried out by comparing the resulting POD-AR baseline solutions with reference products obtained from the PBD-1 scheme described before. Other than the analysis of KBR residuals (which can only be done for GRACE data), this assessment provides

information about the accuracy of POD-AR baseline solutions for the three missions under evaluation and in the three orbital components. For this evaluation, no periods around maneuver execution times have been excluded due to the maneuver estimation strategies employed in the POD-AR and PBD-1 schemes (Table 1).

Figure 4 shows the RMS errors of daily POD-AR baseline solutions for the three test cases and the period under analysis in the three orbital components. Additionally, the assessment of baseline solutions derived from the GNV1B product is also depicted. For the GRACE mission, POD-AR and GNV1B baseline solutions exhibit median RMS error values of 1.6, 2.9 and 1.9 mm and 3.5, 6.5 and 4.7 mm in the radial, along-track and cross-track directions, respectively. The achieved error levels in the along-track component for both solution types are in good accord with the values obtained in the independent baseline validation using KBR observations. For TanDEM-X, the obtained baseline solutions exhibit median RMS error values of 1.4, 2.4 and 2.0 mm in the radial, along-track and cross-track components, while corresponding values of 1.2, 2.1 and 1.4 mm have been obtained for the Swarm A/C baseline. The attained error levels in the along-track direction in the last two missions are indeed close to the previously reported 1D baseline precision values for GRACE using data from before 2010.

Although not explicitly accounted, part of the achieved performance in the above described test cases can be understood by considering some degree of common error cancellation in the formation of POD-AR baseline solutions. While such a feature is most obvious in the observation domain, from a theoretical point of view, common measurement and model errors will result in equal errors in the estimated positions, which can be cancelled when differencing positioning solutions. In practice, however, it is difficult to assume or guarantee observations with correlated errors across independent receivers, as this would imply foremost that the same set of GNSS satellites are tracked by all the spacecraft at every epoch. This difficulty is particularly true in cases with long baselines, different spacecraft designs (and antenna orientations) and dissimilar GNSS receiver architectures. On the other hand, the test cases under consideration in this study are dedicated formation-flying missions with similar or identical designs across all spacecraft. Some of these mission characteristics have likely helped to achieve a certain degree of error cancellation in the differential positioning solutions.

Figure 5 depicts the box-whiskers diagrams of the distribution of daily RMS errors of float (POD) and ambiguity fixed (POD-AR) baseline solutions for the three missions under analysis. In these diagrams, outliers are considered as values below $Q_1 - 1.5 \cdot IQR$ or above $Q_3 + 1.5 \cdot IQR$, where Q_1 , Q_3 and IQR denote the first quartile, the third quartile and inter-quartile range of the distribution, respectively.

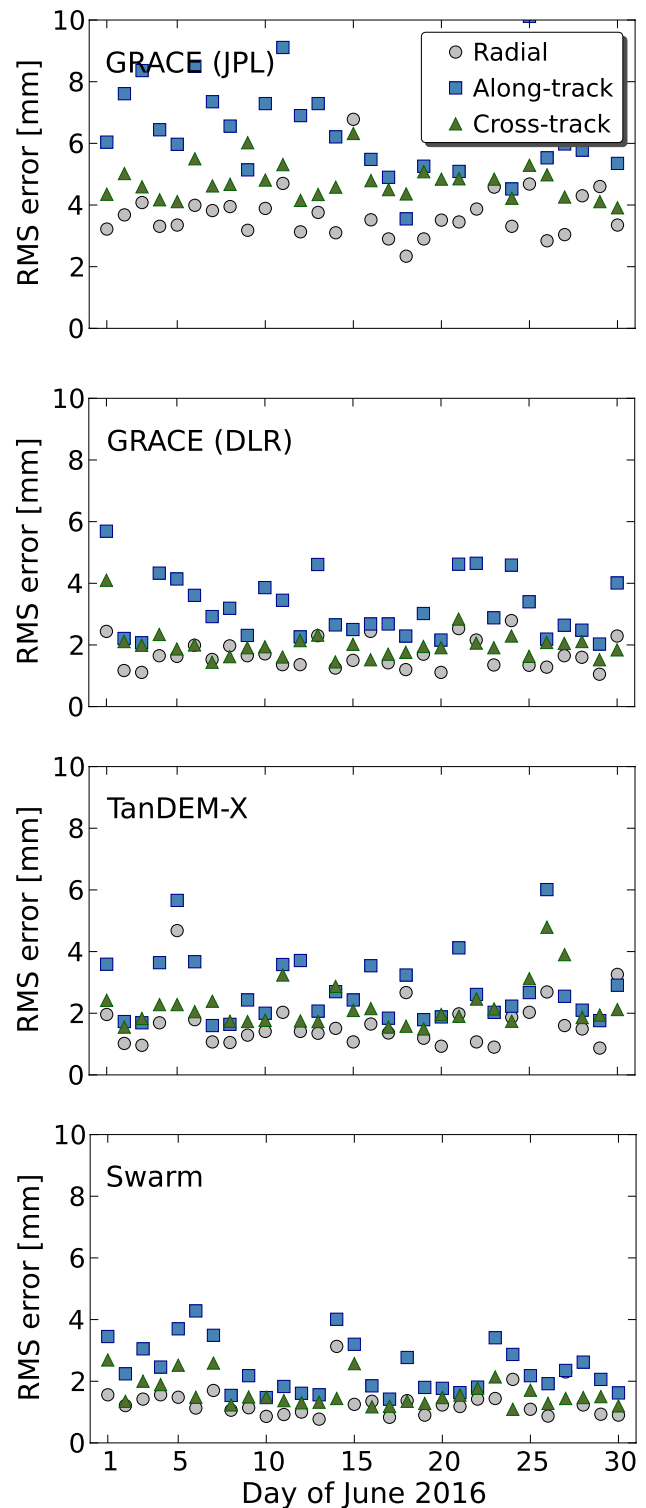


Fig. 4 Assessment of POD-AR baseline solutions for the GRACE, TanDEM-X and Swarm missions in June 2016, using solutions from the PBD-1 scheme as reference. For the GRACE mission, the assessment of baseline solutions derived from the GNV1B product (JPL) is also depicted

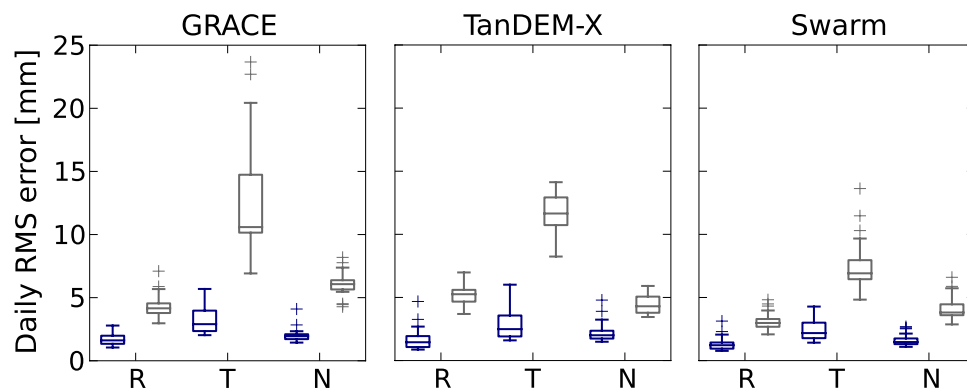


Fig. 5 Box-whiskers diagrams of distributions of daily RMS errors in POD (grey) and POD-AR (blue) baseline solutions for the GRACE, TanDEM-X and Swarm for the period of June 2016 (R: radial, T: along-track, N: cross-track). The box heights and bars inside boxes

denote the inter-quartile range (IQR) and median values of distributions, respectively. Whiskers' lengths represent the maximum and minimum values of distributions. Outliers are identified with plus markers (see text)

Thanks to the sharp geometric constrains provided by fixed ambiguities, POD-AR solutions exhibit an increased stiffness, which results in reduced error levels compared to the traditional float ambiguity POD. This is reflected in the distribution of RMS errors of POD-AR baseline solutions, exhibiting median and 75th percentile values below 5 mm in each axis for all cases, as depicted in Fig. 5. With respect to solutions using float ambiguity POD, a 2- to 4-fold improvement in accuracy can be observed for the three test cases in the individual components of POD-AR baseline solutions. These results may be of particular interest for heterogeneous space missions with baseline accuracy requirements at the sub-centimeter level, such as the planned SAOCOM-CS mission (Montenbruck et al. 2018).

Summary and conclusions

The present study assesses the performance of precise baseline solutions generated from ambiguity fixed single-satellite orbit solutions. It is motivated by concepts of prospective remote sensing missions based on heterogeneous ensembles of multiple spacecraft covering a wide range of inter-satellite distances. In such cases, the application of CDGPS techniques may turn out to be difficult due to dissimilar GPS/GNSS receivers and limitations in the number of commonly tracked satellites. The use of single-satellite orbit solutions for the generation of baseline products may be particularly attractive for such cases due to the possibility of generating each orbit solution in an independent processing chain.

The presented POD-AR baseline solutions inherit the robustness and maturity of POD techniques and improve the accuracy of typical POD products thanks to the application of single-receiver ambiguity fixing. The employed strategy makes use of widelane bias and clock products from

the CNES/CLS analysis center and employs a pass-by-pass widelane and N1 ambiguity resolution scheme. Baseline solutions are then formed based on the generated POD-AR products.

Three test cases have been analyzed, based on flight data from the GRACE, TanDEM-X and Swarm missions using a one-month data set in June 2016. The resulting POD-AR baseline solutions are validated using CDGPS reference solutions with fixed ambiguities and, in case of GRACE, measurements of the K-band ranging system. For all three missions, a better than 5 mm (3D RMS) consistency with the reference solutions is obtained and a 2.6-mm precision (1D, 1σ) is evidenced by the KBR comparison.

Considering different baseline determinations concepts, ambiguity resolved CDGPS solutions achieve consistency levels of better than 1–2 mm (median of daily 1D RMS; see Fig. 2) for missions with identical spacecraft and optimal GPS visibility. As such, they represent the method of choice for formation-flying missions requiring utmost baseline accuracy (e.g., SAR interferometry). Even though the differenced POD-AR solutions discussed in the present study cannot compete with this accuracy, they still show a remarkably good performance of about 1–3 mm (median of daily 1D RMS) under benign mission cases. This is only a factor of 2–3 worse than the CDGPS performance. On the other hand, the differenced POD-AR solutions clearly outperform differenced float-ambiguity POD solutions by a factor 2–4 (see Fig. 5).

The slightly reduced performance of differenced POD-AR solutions compared to CDGPS solutions must, however, be traded against a variety of other benefits. Aside from the flexibility and operational convenience of single- versus multi-satellite processing, the POD-AR scheme can be employed in heterogeneous space missions and promises graceful performance degradation in case of large baselines

or limitations in the set of commonly tracked GPS satellites. It is therefore considered of particular interest for future multi-spacecraft formations or aggregated mission designs requiring sub-cm baseline accuracy but cannot completely benefit from the advantages of short/medium-size baselines, identical spacecraft and common orientation as offered by today's GRACE, TanDEM-X and Swarm missions.

Acknowledgements This study makes use of dedicated GPS orbit, clock and bias products for single-receiver ambiguity resolution, which are made available by the joint CNES/CLS (Centre National d'Etudes Spatiales/Collecte Localisation Satellites) analysis center of the International GNSS Service (IGS). Provision of this community service is greatly appreciated and acknowledged. The authors are grateful to the anonymous reviewers for the provided comments that helped to improve the original manuscript.

References

- Allende-Alba G, Montenbruck O (2016) Robust and precise baseline determination of distributed spacecraft in LEO. *Adv Space Res* 57(1):46–63. <https://doi.org/10.1016/j.asr.2015.09.034>
- Allende-Alba G, Montenbruck O, Ardaens J-S, Wermuth M, Hugentobler U (2017) Estimating maneuvers for precise relative orbit determination using GPS. *Adv Space Res* 59(1):45–62. <https://doi.org/10.1016/j.asr.2016.08.039>
- Barbier C, Derauw D, Orban A, Davidson MWJ (2014) Study of a passive companion microsatellite to the SAOCOM-1B satellite of Argentina, for bistatic and interferometric SAR applications. In: Proceedings SPIE 9241, Sensors, Systems and Next-Generation Satellites XVII, 11 Nov, Amsterdam, Netherlands, <https://doi.org/10.1117/12.2066307>
- Bertiger WI, Bar-Sever YE, Christensen EJ, Davis ES, Guinn JR et al (1994) GPS precise tracking of TOPEX/POSEIDON: results and implications. *J Geophys Res Oceans* 99(C12):24449–24464. <https://doi.org/10.1029/94JC01171>
- Bertiger WI, Desai SD, Haines B, Harvey N, Moore AW et al (2010) Single receiver phase ambiguity resolution with GPS data. *J Geodesy* 84(5):327–337. <https://doi.org/10.1007/s00190-010-0371-9>
- Bock H, Jäggi A, Beutler G, Meyer U (2014) GOCE: precise orbit determination for the entire mission. *J Geodesy* 88(11):1047–1060. <https://doi.org/10.1007/s00190-014-0742-8>
- Bock H, Jäggi A, Fernández J, Escobar D, Ayuga F et al (2017) Sentinel-1A—first precise orbit determination results. *Adv Space Res* 60(5):879–892. <https://doi.org/10.106/j.asr.2017.05.034>
- Börner T, López Dekker P, Krieger G, Bachmann M, Moreira A et al. (2014) Passive interferometric ocean currents observation synthetic aperture radar (PICOSAR). In: Sandau R, Röser H-P, Valenzuela A (eds) Small satellites for earth observation—missions & technologies, 1(4):pp 53–60
- Dach R, Brockmann E, Schaer S, Beutler G, Meindl M et al (2009) GNSS processing at CODE: status report. *J Geodesy* 83(3–4):353–365. <https://doi.org/10.1007/s00190-008-0281-2>
- Doornbos E (2012) Thermospheric density and wind determination from satellite dynamics. Springer Heidelberg, ISBN: 978-3-642-25128-3
- Eanes RJ, Bettadpur S (1996) The CSR 3.0 global ocean tide model: diurnal and semi-diurnal ocean tides from TOPEX/POSEIDON altimetry, CSR-TM-96-05, University of Texas at Austin
- Flechtner F, Morton P, Watkins M, Webb F (2014) Status of the GRACE Follow-on mission. In Marti, U. (ed), Gravity, Geoid and Height Systems: Proceedings of the IAG Symposium GGHS2012, 9–12 Oct 2012, Venice, Italy
- Friis-Christensen E, Lühr H, Knudsen D, Haagmans R (2008) Swarm—an earth observation mission investigating geospace. *Adv Space Res* 41(1):210–216. <https://doi.org/10.1016/j.asr.2006.10.008>
- Hackel S, Montenbruck O, Steigenberger P, Balss U, Gisinger C et al (2017) Model improvements and validation of TerraSAR-X precise orbit determination. *J Geodesy* 91(5):547–562. <https://doi.org/10.1007/s00190-016-0982-x>
- Haines B, Bar-Sever YE, Bertiger WI, Desai S, Willis P (2004) Once-centimeter orbit determination for Jason-1: new GPS-based strategies. *Mar Geodesy* 27(1–2):299–318. <https://doi.org/10.1080/01490410490465300>
- Hatch R (1982) The synergism of GPS code and carrier measurements. In: Proceedings of the third international symposium on satellite Doppler positioning at physical sciences laboratory of New Mexico State University, vol 2, pp 1213–1231
- Homer J, Longstaff ID, Callaghan G (1996) High resolution 3-D SAR via multi-baseline interferometry. In: Proceedings of the IEEE Geoscience and Remote Sensing Symposium, Lincoln, NE, <https://doi.org/10.1109/IGARSS.1996.516478>
- Hueso González J, Antony W, Bachmann JM, Krieger M, Zink G, M., et al (2012) Bistatic system and baseline calibration in TanDEM-X to ensure the global digital elevation model quality. *ISPRS J Photogrammetry Rem Sens* 73:3–11. <https://doi.org/10.1016/j.isprsjprs.2012.05.008>
- Jäggi A, Hugentobler U, Bock H, Beutler G (2007) Precise orbit determination for GRACE using undifferenced or doubly differenced GPS data. *Adv Space Res* 39(10):1612–1619. <https://doi.org/10.1016/j.asr.2007.03.012>
- Kang Z, Tapley B, Bettadpur S, Ries J, Nagel P et al (2006) Precise orbit determination for the GRACE mission using only GPS data. *J Geodesy* 80(6):322–331. <https://doi.org/10.1007/s00190-006-0073-5>
- Knocke PC, Ries JC, Tapley BD (1988) Earth radiation pressure effects on satellites. In: AIAA/AAS astrodynamics conference, 15–17 Aug, Minneapolis, MN, pp 577–587
- Krieger G, Moreira A. Spaceborne bi- and multi-static SAR: potential and challenges (2006) IEEE Proceedings – Radar, Sonar and Navigation, 153(3):184–198. <https://doi.org/10.1049/ip-rsn:2004111>
- Krieger G, Moreira A (2008) Spaceborne interferometric and multi-static SAR systems. In: Cherniakov M (ed), Bistatic radar: Emerging Technology, New York: Wiley, pp 95–158
- Krieger G, Moreira A, Fiedler H, Hajnsek I, Werner M, Younis M, Zink M (2007) TanDEM-X: a satellite formation for high-resolution SAR interferometry. *IEEE Trans Geosci Remote Sens* 45(11):3317–3340. <https://doi.org/10.1109/TGRS.2007.900693>
- Krieger G, Zink M, Bachmann M, Bräutigam B, Schulze D et al (2013) TanDEM-X: a radar interferometer with two formation-flying satellites. *Acta Astronaut* 89:83–98. <https://doi.org/10.1016/j.actastro.2013.03.008>
- Kroes R, Montenbruck O, Bertiger W, Visser P (2005) Precise GRACE baseline determination using GPS. *GPS Solutions* 9(1):21–31. <https://doi.org/10.1007/s10291-004-0123-5>
- Laurichesse D, Mercier F (2007) Integer ambiguity resolution on undifferenced GPS phase measurements and its application to PPP. In: Proceedings of the ION GNSS 2007, pp 839–848
- Laurichesse D, Mercier F, Berthias JP, Broca P, Cerri L (2009) Integer ambiguity resolution on undifferenced GPS phase measurements and its application to PPP and satellite precise orbit determination. *Navigation* 56(2):135–149. <https://doi.org/10.1002/j.2161-4296.2009.tb01750.x>
- Loyer S, Perosanz P, Mercier F, Capdeville H, Marty JC (2012) Zero-difference GPS ambiguity resolution at CNES-CLS IGS analysis center. *J Geodesy* 86(11):991–1003. <https://doi.org/10.1007/s00190-012-0559-2>

- Mao X, Visser P, van den IJssel J (2017) Impact of GPS antenna phase center and code residual variation maps on orbit and baseline determination of GRACE. *Adv Space Res* 59(12):2987–3002. <https://doi.org/10.1016/j.asr.2017.03.019>
- Mayer-Gürr T, Pail R, Schuh WD, Kusche J, Baur O et al. (2012) The new combined satellite only model GOCO03s. In: International Symposium on Gravity, Geoid and Height Systems, Venice, Italy
- Melbourne W (1985) The case for ranging in GPS based geodetic systems. In: Goad C (ed) Proc. 1st Int. Symp. on Precise Positioning with the Global Positioning System, NOAA, pp 373–386
- Milani A, Nobili AM, Farinella P (1987) Non-gravitational perturbations and satellite geodesy. Adam Hilger Ltd Bristol, ISBN: 0-85274-538-9
- Montenbruck O, Gill E (2005) Satellite orbits. Springer Heidelberg
- Montenbruck O, Garcia-Fernandez M, Yoon Y, Schön S, Jäggi A (2009) Antenna phase center calibration for precise positioning of LEO satellites. *GPS Solutions* 13:23–34. <https://doi.org/10.1007/s10291-008-0094z>
- Montenbruck O, Wermuth M, Kahle R (2011) GPS based relative navigation for the TanDEM-X mission – first flight results. *Navigation* 58(4):293–304. <https://doi.org/10.1002/j.2161-4296.2011.tb02587.x>
- Montenbruck O, Hackel S, Jäggi A (2017) Precise orbit determination of the Sentinel-3A altimetry satellite using ambiguity-fixed GPS carrier phase observations. *J Geodesy*. <https://doi.org/10.1007/s00190-017-1090-2>
- Montenbruck O, Allende-Alba G, Rosello J, Tossaint M, Zangerl F (2018) Precise orbit and baseline determination for the SAOCOM-CS bistatic radar mission. *Navigation* 65(1):15–24. <https://doi.org/10.1002/navi.216>
- Moreira A, Krieger G, Hajnsek I, Papathanassiou KP, Younis M et al (2015) Tandem-L: a highly innovative bistatic SAR mission for global observations of dynamic processes on the earth's surface. *IEEE Geosci Rem Sens Magazine* 3(2):8–23. <https://doi.org/10.1109/MGRS.2015.2437353>
- Picone JM, Hedin AE, Drob DP, Aikin AC (2002) NRLMSISE-00 empirical model of the atmosphere: statistical comparisons and scientific issues. *J Geophys Res Space Phys* 107(A12):SIA 15-1-SIA pp 15–16. <https://doi.org/10.1029/2002JA009430>
- PODAAC (2017) Physical oceanography distributed active archive center – gravity recovery and climate experiment. <http://podaac.jpl.nasa.gov/allData/grace>. Last accessed November 2017
- Priestley KJ, Smith GL, Thomas S, Cooper D, Lee RB et al (2011) Radiometric performance of the CERES earth radiation budget climate record sensors on the EOS Aqua and Terra spacecraft through April 2007. *J Atmos Oceanic Technol* 28(1):3–21. <https://doi.org/10.1175/2010JTECHA1521.1>
- Qiao L, Rizos C, Dempster A (2011). Satellites Orbit Design and Determination for the Australian Garada Project. Proc. ION GNSS 2011, Portland, Oregon
- Schmid R, Dach R, Collilieux X, Jäggi A, Schmitz M, Dilssner F (2016) Absolute IGS antenna phase center model igs08.atx: status and potential improvements. *J Geodesy* 90(4):343–364. <https://doi.org/10.1007/s00190-015-0876-3>
- Sentman LH (1961) Free molecule flow theory and its application to the determination of aerodynamic forces. Lockheed Missile and Space Co., Sunnyvale, TR LMSC-448514, AD 265–409
- Shampine LF, Gordon MK (1975) Computer solution of ordinary differential equations: the initial value problem. W.H. Freeman, San Francisco
- Sutton EK (2009) Normalized force coefficients for satellites with elongated shapes. *J Spacecraft Rockets* 46(1):112–116. <https://doi.org/10.2514/1.40940>
- Tapley BD, Bettadpur S, Watkins M, Reigber C (2004) The gravity recovery and climate experiment: mission overview and early results. *Geophys Res Lett*, 31(9), <https://doi.org/10.1029/2004GL019920>
- Teunissen PJG (1994) The least-squares ambiguity decorrelation adjustment: a method for fast GPS integer ambiguity estimation. *J Geodesy* 70(1–2):65–82. <https://doi.org/10.1007/BF00863419>
- Teunissen PJG, Khodabandeh A (2015) Review and principles of PPP-RTK methods. *J Geodesy* 89(3):217–240. <https://doi.org/10.1007/s00190-014-0771-3>
- van Barneveld PWL (2012) Orbit determination of satellite formations. PhD Thesis, Technische Universiteit Delft. ISBN: 9778-94-6191-546-7
- van den IJssel J, Visser P, Patiño Rodriguez E (2003) Champ precise orbit determination using GPS data. *Adv Space Res* 31(8):1889–1895. [https://doi.org/10.1016/S0273-1177\(03\)00161-3](https://doi.org/10.1016/S0273-1177(03)00161-3)
- van den IJssel J, Encarnação J, Doornbos E, Visser P (2015) Precise science orbits for the Swarm satellite constellation. *Adv Space Res* 56(6):1042–1055. <https://doi.org/10.1016/j.asr.2015.06.002>
- Wu SC, Yunck TP, Thornton CL (1991) Reduced-dynamic technique for precise orbit determination of low earth satellites. *J Guid Control Dyn* 14(1):24–30. <https://doi.org/10.2514/3.20600>
- Wu JT, Wu SC, Hajj G, Bertiger WI, Lichten SM (1993) Effects of antenna orientation on GPS carrier phase. *Manuscripta Geodaetica* 18(2):91:98
- Wübbena G (1985) Software developments for geodetic positioning with GPS using TI 4100 code and carrier measurements. In: Goad C (ed) Proc. 1st Int. Symp. on Precise Positioning with the Global Positioning System, NOAA, pp 403–412
- Yunck TP, Wu SC, Wu JT, Thornton CL (1990) Precise tracking of remote sensing satellites with the Global Positioning System. *IEEE Trans Geosci Remote Sens* 28(1):108–116. <https://doi.org/10.1109/36.45753>

Gerardo Allende-Alba is a scientific staff member of the GNSS technology and navigation group at DLR's German Space Operations Center. In 2012, he received his M.Sc. in earth oriented space science and technology from Munich University of Technology. His current research activities are focused on precise orbit and baseline determination using GNSS carrier phase observations.

Oliver Montenbruck is head of the GNSS technology and navigation group at DLR's German Space Operations Center. His research activities comprise spaceborne GNSS receiver technology, autonomous navigation systems, spacecraft formation flying and precise orbit determination as well as new constellations and multi-GNSS processing. Oliver Montenbruck presently chairs the multi-GNSS working group of the International GNSS Service and coordinates the performance of the MGEX Multi-GNSS Experiment.

Stefan Hackel works as engineer at the flight dynamic section at DLR's German Space Operations Center. He received his M.Sc. degree from Munich's University of Technology in 2012 and is currently doing his PhD in precise orbit determination of low-earth spacecraft, where refined dynamical models and integer ambiguity fixing of GPS observations are key interests.

Michel Tossaint is a system engineer at the earth observation-future mission division at ESTEC for the European Space Agency (ESA), the Netherlands. He graduated M.Sc. in aerospace engineering from Delft University of Technology in 1997. In 2001 he joined ESA working on topics like EGNOS design and Galileo experimentation. From 2008 he was navigation technical officer in the Galileo project and evolution program working on Galileo second generation design.